Function of a Conserved Loop of the β-Domain, Not Involved in Thiamin Diphosphate Binding, in Catalysis and Substrate Activation in Yeast Pyruvate Decarboxylase†

Ebenezer Joseph,‡,§ Wen Wei,‡,§ Kai Tittmann,|| and Frank Jordan*,§

Department of Chemistry, Rutgers, the State University of New Jersey, Newark, New Jersey 07102, and Department of Biochemistry, Martin Luther University, Halle, Germany

Received August 1, 2006; Revised Manuscript Received September 13, 2006

ABSTRACT: The X-ray crystal structure of pyruvamide-activated yeast pyruvate decarboxylase (YPDC) revealed a flexible loop spanning residues 290 to 304 on the β-domain of the enzyme, not seen in the absence of pyruvamide, a substrate activator surrogate. Site-directed mutagenesis studies revealed that residues on the loop affect the activity, with some residues reducing k_{cat}/K_m by at least 1000-fold. In the pyruvamide-activated form, the loop located on the β domain can transfer information to the active center thiamin diphosphate (ThDP) located at the interface of the α and γ domains. The sigmoidal v_0−[S] curve with wild-type YPDC attributed to substrate activation is modulated for most variants, but is not abolished. Pre-steady-state stopped-flow studies for product formation on these loop variants provided evidence for three enzyme conformations connected by two transitions, as already noted for the wild-type YPDC at pH 5.0 [Sergienko, E. A., and Jordan, F. (2002) *Biochemistry 41*, 3952−3967]. ^{1}H NMR analysis of the intermediate distribution resulting from acid quench [Tittmann et al. (2003) *Biochemistry 42*, 7885−7891] with all YPDC variants indicated that product release is rate limiting in the steady state. Apparently, the loop is not solely responsible for the substrate activation behavior, rather it may affect the behavior of residue C221 identified as the trigger for substrate activation. The most important function of the loop is to control the conformational equilibrium between the "open" and "closed" conformations of the enzyme identified in the pyruvamide-activated structure [Lu et al. (2000) *Eur. J. Biochem. 267*, 861−868].

The X-ray structure of yeast pyruvate decarboxylase [YPDC,[1] carries out a thiamin diphosphate (ThDP)-dependent decarboxylation of pyruvate to acetaldehyde (*1*, *2*)] revealed a structural change on addition of the substrate activator surrogate pyruvamide (a pyruvate analogue that cannot be decarboxylated) (*3*). In the absence of pyruvate or pyruvamide, YPDC exists in form A, sometimes called the unactivated form; in the presence of pyruvamide, the YPDC tetramer is converted to form B, sometimes called the activated form. In form A, four monomers are assembled in a 222 symmetry with two dimers loosely packed together. In form B, the two dimers are twisted by 6.3−8.2° in the relative orientation of the β domain in one subunit to the β domain in the other subunit, while the orientation of the other two domains (α and γ, which jointly create the ThDP binding site and supply the active center catalytic residues) remains similar in the A and B forms. With pyruvamide present, one side of the dimer−dimer interfaces is packed much tighter than the other side and the 222 symmetry is totally abolished (Figure 1). Unlike in form A, where all four active sites are equivalent, in form B of YPDC, two active sites on the tightly packed side are closed (called C for closed subunit) and two on the other side are exposed (called O for open subunit) to the solvent as a consequence of the structural rearrangement (*3*).

Two loop regions (encompassing residues 104−113 and 290−301) were found to have no interpretable electron density in the form A structure (*1*, *2*), indicating that these regions are disordered and highly flexible. Interestingly, in the form B structure (*3*), loop 290−301 becomes organized in the subunit on the side of the tetramer where dimers are tightly packed (the closed C subunit) and the loop 104−113 is ordered in the subunit on the other side of the tetramer where dimers are loosely packed (the opened O subunit). Therefore, these two regions may have importance in the substrate activation of YPDC, reflected by a sigmodial v_0−[S] plot (*4*, *5*), with a Hill coefficient near 2.0. The spatial relationship of the loop to the active center ThDP is shown in Figure 2. Evidence for the substrate activation pathway explored by the Rutgers group (*6*−*9*) suggests that formation of a hemithioketal between C221 (β domain) and pyruvate enables the negative charge to reach H92 (α domain) forming an ion pair. This actuates transfer of information via E91 onto W412 (γ domain, part of a loop that includes residues

† This work was supported at Rutgers by Grant NIH GM-50380 and at Halle by Research Grant 0126FP/0705M by the Ministry of Education at Saxony-Anhalt.

* Corresponding author. Tel: 973-353-5470. Fax: 973-353-1264. E-mail: frjordan@newark.rutgers.edu.

‡ These authors contributed equally to the work here reported.

§ Rutgers, the State University of New Jersey.

|| Martin Luther University.

[1] Abbreviations: ThDP, thiamin diphosphate; PDC, pyruvate decarboxylase; YPDC, yeast pyruvate decarboxylase; HEThDP, C2α-hydroxyethylthiamin diphosphate, the acetaldehyde·ThDP adduct; LThDP, C2α-lactylthiamin diphosphate, the pyruvate·ThDP adduct.

10.1021/bi0615588 CCC: $33.50
Published on Web 10/25/2006

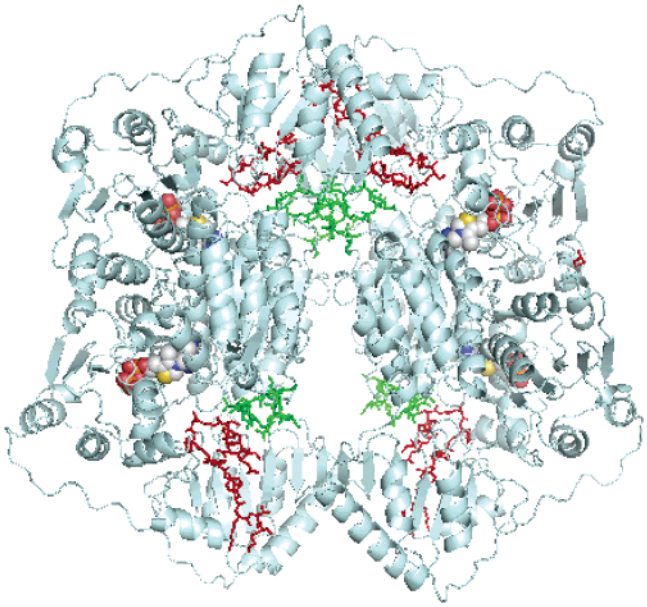

FIGURE 1: The pyruvamide-activated structure of YPDC (*3*). Upper subunits are closed. Lower ones are open. The 290−301 loop is red; the 104−113 loop is green; ThDP in space-filling presentation.

410−415) to G413 (forms a conserved hydrogen bond with the amino group of ThDP), to S414 and to I415 (this residue was termed the conformational pivot ensuring the stabilization of the reactive "V" conformation of ThDP).

Previous evidence for the importance of this loop was obtained from studies on the autoregulation of YPDC (*10*), that identified the mutant yeasts *pdc-8* (with a D291N substitution) and *pdc-803* (with a S296ΔF297Δ deletion). Using site directed mutagenesis, two variants D291N and S296ΔF297Δ were created to mimic these genetic findings (*11*, *12*). Although these two variants displayed extremely low activity (0.0022 U/mg for *pdc-8* and 0.0016 U/mg for *pdc-803*), compared to 50−60 U/mg for wild-type enzyme, no structure−function explanation had been provided. We here report detailed studies of loop 290−301. Among the 12 residues stretching from 290 to 301, D291, T294, N293, S298, and S300 were selected and singly substituted by alanine since an examination of this loop (Figure 3) revealed some interesting interactions in which these particular residues might be involved. Steady-state kinetic constants were determined for each variant in the pH range of activity (5.1−7.5). In addition, mechanistic studies were carried out to elucidate the effects of these substitutions, distant from the active center, on events taking place at the active center. The results provide insight to the role of the β domain, not directly involved in binding ThDP, unlike the α and γ domains. Studies were also carried out for the L111 residue from loop 104−113. The L111A, L111V, and L111Q YPDC variants were constructed, and their kinetic parameters were determined in the same pH range (5.1−7.5).

EXPERIMENTAL PROCEDURES

Materials. The QuikChange site-directed mutagenesis kit was from Stratagene (La Jolla, CA). The Wizard 373 DNA purification system was from Promega Inc. (Madison, WI). Primers were synthesized by Integrated DNA Technologies, Inc. (Coralville, IA). Talon metal affinity resin was from Clontech Laboratories, Inc. (Palo Alto, CA). All chemicals were purchased from Sigma (St. Louis, MO) or USB (Cleveland, OH). The BL21 (DE3) competent cells were from Novagen Inc. (Madison, WI).

Construction of D291A, N293A, T294A, S298A, S300A, L111A, L111V, and L111Q Variants of YPDC. Site-directed mutagenesis experiments to produce the D291A, N293A, T294A, S298A, S300A, L111A, L111V, and L111Q variants used the QuikChange site-directed mutagenesis kit following the manufacturer's instructions. The plasmid of His_6−wild-type YPDC was used as the template for all variants (*13*). The primers designed for the mutagenesis experiment are listed below (the new codons in place of the original codons are typed in bold face and the mutated sites are underlined):

D291A1	5'-GTGCTTTGTTGTCT**GC**TTTCAACACCGGTTCTTTC-3'
D291A2	5'-GAAAGAACCGGTGTTGAAA**GC**AGACAACAAAGCAC-3'
N293A1	5'-CTTTGTTGTCTGATTTC**GCC**ACCGGTTCTTTCT-3'
N293A2	5'-GAGAAAGAACCGGT**GGC**GAAATCAGACAACAAAG-3'
T294A1	5'-GTTGTCTGATTTCAAC**GCC**GGTTCTTTCTCTTAC-3'
T294A2	5'-GTAAGAGAAAGAACC**GGC**GTTGAAATCAGACAAC-3'
S298A1	5'-CAACACCGGTTCTTTC**GCT**TACTCTTACAAGACC-3'
S298A2	5'-GGTCTTGTAAGAGTA**AGC**GAAAGAACCGGTGTTG-3'
S300A1	5'-CACCGGTTCTTTCTCTTAC**GCT**TACAAGACCAAG-3'
S300A2	5'-CTTGGTCTTGTAA**GC**GTAAGAGAAAGAACCGGTG-3'
L111A1	5'-CAAGCTAAGCAA**GCG**TTGTTGCACCACACCTTAG-3'
L111A2	5'-CTAAGGTGTGGTGCAACAA**CGC** TTGCTTAGCTTG-3'
L111V1	5'-CAAGCTAAGCAA**GTG**TTGTTGCACCACACCTTAG-3'
L111V2	5'-CTAAGGTGTGGTGCAACAA**CAC** TTGCTTAGCTTG-3'
L111Q1	5'-CAAGCTAAGCAA**CAG**TTGTTGCACCACACCTTAG-3'
L111Q2	5'-CTAAGGTGTGGTGCAACAA**CTG** TTGCTTAGCTTG-3'

The *Escherichia coli* strain BL21 (DE3) cells were transformed with the mutated plasmids, and the cells were allowed to grow on LB-ampicillin agar plate overnight (>16 h).

DNA Sequencing. Desired mutations were confirmed by means of fluorescence-based DNA sequencing. Plasmids of the variants extracted from 10 mL of culture were sequenced by use of the Dye Terminator Cycle Sequencing Ready Reaction kit on an ABI 373 sequencer.

Enzyme Expression and Purification. Single colonies of the cells were incubated in LB medium containing 50 μg/mL ampicillin at 37 °C with shaking at 300 rpm and induced with 0.5 mM IPTG when A_{650} reached 1.0−1.2. After 4−5 h of induction, the cells were collected, washed with 20 mM KPi by centrifugation, and stored at −20 °C.

Since the plasmid of His_6 wild-type YPDC was used as the template for mutagenesis, all variants have a His_6 tag attached to their C-terminus. The procedure for purification of His_6 tag YPDC variants is identical to the purification of His_6 tag wild-type YPDC described elsewhere (*13*).

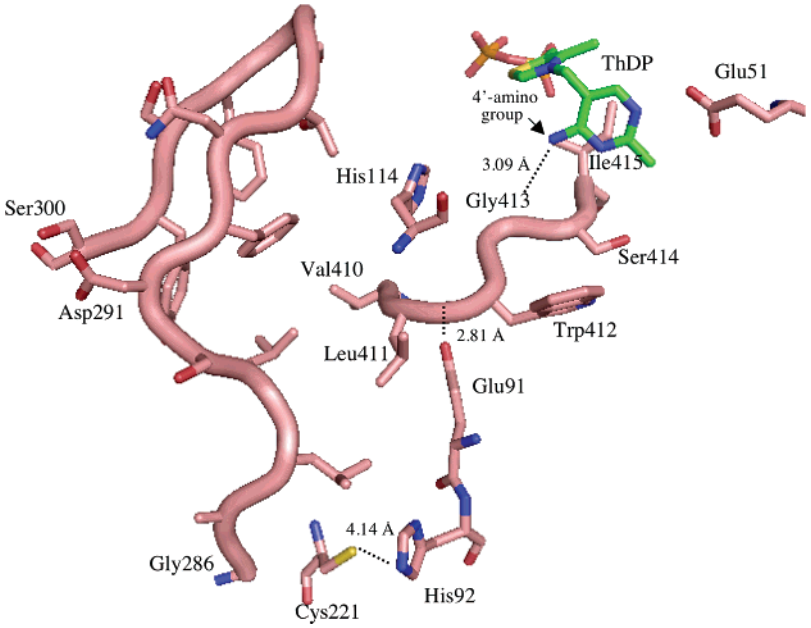

FIGURE 2: Pictorial representation of the connectivity of the regulatory site (Cys221) with respect to the loop 291−300 and the active site. The pdb file 1qpb (*3*) was used to generate the model.

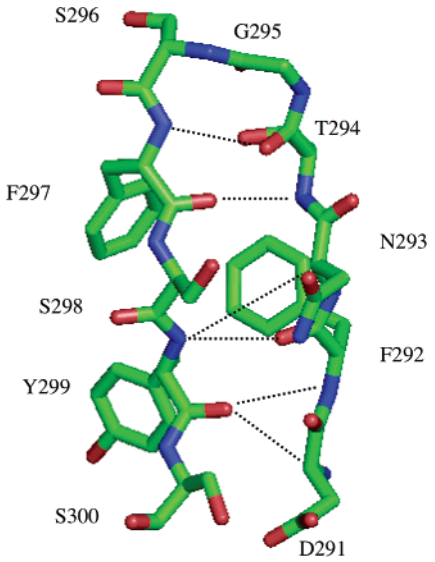

FIGURE 3: Pictorial representation of the loop residues in pyruvamide activated YPDC. "**...**" represents hydrogen bonds formed within the loop giving rise to 6 H-bonds within the loop. The pdb file 1qpb (*3*) was used to generate the model.

Steady-State Kinetic Analysis. The NADH/ADH coupled assay was used to determine the enzyme activity (*14*) monitoring the depletion of NADH at 340 nm by using a COBAS−BIO automatic centrifugal analyzer (Roche Diagnostics Corp., Indianapolis, IN). A triple buffer (50 mM MES, 100 mM Tris, 50 mM acetic acid with 2 mM $MgCl_2$, 1 mM ThDP, and 1 mM EDTA) provided constant ionic strength in the entire pH range. The v_0−[S] data were fitted to the Hill equations:

$$v_0/[E_0] = k_{cat}[S]^n/(S_{0.5}{}^n + [S]^n) \quad (1)$$

$$v_0/[E_0] = k_{cat}[S]^n/\{S_{0.5}{}^n + [S]^n(1 + [S]/K_i)\} \quad (2)$$

Data that exhibited no substrate inhibition were fitted to eq 1 while data showing substrate inhibition were fitted to eq 2 using the Sigma Plot program from SPSS, leading to the values for k_{cat}, $S_{0.5}$, $k_{cat}/S_{0.5}$, $k_{cat}/S_{0.5}{}^n$, and n_H (the Hill coefficient).

Differential scanning calorimetry measurements were carried out using the Perkin-Elmer Pyris 1 calorimeter at a scan rate of 1 °C/min in 20 mM MES buffer (pH 6.0). Samples (20 mg/mL) were scanned from 25 to 95 °C, and the midpoint melting temperature (T_m) was determined.

Determination of the Pre-Steady-State Kinetic Parameters. The progress curves of product (acetaldehyde) formation were recorded via a yeast alcohol dehydrogenase/NADH coupled assay (*14*) on an Applied Photophysics SX18 MV stopped-flow spectrophotometer (Leatherhead, U.K.). Pyruvate decarboxylase (wild type, 10−84 μg/mL or 0.17−1.43 μM active sites, or variants) was premixed with NADH (0.3 mM) and ADH (350 units/mL). This solution was then mixed in a 1:1 ratio with pyruvate at different concentrations dissolved in the same buffer. The temperature was maintained at 31 °C with a Lauda MGW water bath. The absorbance change at 340 nm was measured with a light path of either 2 or 10 mm. The data (total of 4000 points) were transferred to a PC and treated with the SigmaPlot software according to eq 3:

$$P = \frac{k_{tr2}(v_2 - v_0) + k_{tr1}(v_0 - v_1)}{k_{tr1}(k_{tr1} - k_{tr2})}[1 - \exp(-k_{tr1}t)] + \frac{(v_1 - v_2)k_{tr1}}{(k_{tr1} - k_{tr2})k_{tr2}}(1 - \exp(-k_{tr2}t)] + v_2t \quad (3)$$

where v_0, v_1, and v_2 depict activities of three distinct enzyme states, E_0, E_1, and E_2. The rate constant k_{tr1} pertains to the transition from E_0 to E_1 and k_{tr2} to the transition from E_1 to E_2. When we wished to compare the results with those given by the earlier model involving just two enzyme states, eq 4 was used:

$$P = \frac{v_0 - v_1}{k_{tr1}}[1 - \exp(-k_{tr1}t)] + v_1 t \qquad (4)$$

where all parameters have the same meaning as in eq 3. Equation 3 leads to eq 4 by setting $v_1 = v_2$. These equations were developed (*15*) to account for the complex activation behavior observed with wild-type YPDC at pH values different from that in the optimal range.

The data were also treated with the equations derived by Krieger et al. (*16*) where similar issues on activation were also found with PDC from *Kluyveromyces lactis*.

Rapid chemical quench experiments were carried out in a Kintek instrument. Enzyme, 15 mg/mL, with 1:1 molar ratio of active sites to ThDP is placed in a 1 mL syringe and injected onto sample loop A at the port indicating sample A, and 100 mM pyruvate (in 0.1 M MES, pH 6.0) is injected onto sample loop B. MES buffer, pH 6.00, is injected into drive syringes A and B while quench solution (12.5% trichloroacetic acid, 1 M HCl, 50% D_2O) is injected into drive syringe C. Via the computer, the requisite time and the loop position could be set. A 1.5 mL Eppendorf tube with a pinhole on top is held at the exit line to collect the quenched reaction sample. The experiment is repeated if larger sample volume is needed. The solution was centrifuged for 5 min at 14 000 rpm to precipitate the protein, and the supernatant was used for intermediate analysis by NMR.

For slower reactions, the quenching was performed manually. Pyruvate (120 μL of 100 mM) was added to 120 μL of enzyme. The reaction mixture was quenched with 120 μL of quench solution (12.5% trichloroacetic acid, 1 M HCl, 50% D_2O). The mixture was centrifuged for 5 min at 14 000 rpm, and the NMR spectrum of the supernatant was recorded.

Determination of Microscopic Rate Constants. The microscopic rate constants are determined using the following formulas (*17*):

$$[\text{ThDP}]/[\text{LThDP}] = k_3/k_2 = a$$

$$[\text{ThDP}]/[\text{HEThDP}] = k_{45}/k_2 = b$$

$$k_{cat} = (k_2k_3k_{45})/\{(k_2k_{45}) + (k_2k_{45}) + (k_3k_{45})\}$$

$$k_2 = k_{cat}(a + b + ab)/ab$$

$$k_3 = k_{cat}(a + b + ab)/b$$

$$k_{45} = k_{cat}(a + b + ab)/a$$

where k_2 and k_3 correspond to formation of LThDP and decarboxylation, respectively, while the rate constant k_{45} is a composite including the unimolecular forward rate constant for protonation of the enamine/C2α-carbanion (step 4) and elimination of acetaldehyde (step 5); all rate constants and steps refer to the numbering in Scheme 1.

RESULTS

Construction of the Variants. The residues D291, N293, T294, S298, S300 of YPDC were successfully replaced by alanine, while L111 was replaced by alanine, valine, and glutamine via site-directed mutagenesis, yielding single amino acid-substituted variants D291A, N293A, T294A, S298A, S300A, L111A, L111V, and L111Q. All desired mutations were confirmed by DNA sequencing (*18*).

Expression and Purification. All variants could be overexpressed in the BL21(DE3) cells after IPTG induction and purified to apparent homogeneity (SDS−PAGE) with a subunit molecular weight near 60 000, somewhat higher than non-His_6 tag YPDC due to the C-terminal fusion protein including the six histidines.

(a) Steady-State Kinetic Analysis for Loop 291−301 Variants

The steady-state parameters of variants D291A, N293A, T294A, S298A, and S300A were determined in the pH range of 5.1−7.5 (5.4−7.5 for N293A) and are compared to those of the wild-type YPDC at pH 6.0 in Table 1. The plots of the pH dependence of the parameters for the five variants are presented in Supporting Information Figures S1.A−E and Supporting Information Tables S1.A−E.

Effects of Substitution on k_{cat}. Substitutions at D291, N293, T294, and S298 dramatically reduce the k_{cat} of YPDC by 30−18000-fold, suggesting that these four residues function in the stabilization of transition states of the steps after substrate binding and most likely starting with the decarboxylation of LThDP. The pH profiles for k_{cat} of all five variants are similar to that observed with wild-type YPDC. The k_{cat} reaches its optimum value at pH 6.6 in wild-type YPDC while the pH optima of k_{cat}s in all five variants are slightly shifted to the alkaline side by about 0.3 unit, to approximately pH 6.9. The k_{cat} of S300A reaches 91% of wild-type YPDC activity at pH 6.0, and the activity is virtually unaffected by this substitution.

Effects of Substitution on $k_{cat}/S_{0.5}$ and $k_{cat}/S_{0.5}^n$. On the basis of the Rutgers model (*15*) for multiple substrate binding, the term $k_{cat}/S_{0.5}^n$ approximately accounts for transition state energies starting from binding the first substrate and terminating with the first irreversible step, decarboxylation. In the earlier Schellenberger−Hübner−Showen (SHS) model for the wild-type YPDC (*19*), which assumes two substrate-binding sites per subunit, the corresponding term is k_{cat}/A. The quantity $k_{cat}/S_{0.5}$ approximately represents the transition state energy of steps starting with the E·S complex (probably after the substrate activation step) and culminating with decarboxylation (*15*).

Substitution on S300 had no effect on $k_{cat}/S_{0.5}$; the value for the S300A variant is even greater than that of wild-type YPDC. Substitutions at the remaining four positions profoundly affected the $k_{cat}/S_{0.5}$ of YPDC by reducing this parameter 200−6000-fold. All five variants display bell shaped behavior in the $k_{cat}/S_{0.5}$−pH plots. The N293A and S300A variants reach their optimal $k_{cat}/S_{0.5}$ value at pH 6.0, as does wild-type YPDC. The optimal $k_{cat}/S_{0.5}$ was shifted to ∼pH 5.4 for the D291A and to ∼pH 6.6 for the T294A and the S298A, indicating perturbation on the active center acid−base groups participating in steps culminating with decarboxylation in the D291A, T294A, and S298A variants.

At pH 6.0, the variants show a 500−17000-fold decrease in $k_{cat}/S_{0.5}^n$ compared to the k_{cat}/A of wild type, again with the exception of S300A which has slightly greater value than wild type.

Effects of Substitution on $S_{0.5}$. $S_{0.5}$s for D291A, N293A, and S300A are similar to that of wild-type YPDC while $S_{0.5}$s

Scheme 1: Mechanism of Pyruvate Decarboxylase, YPDC

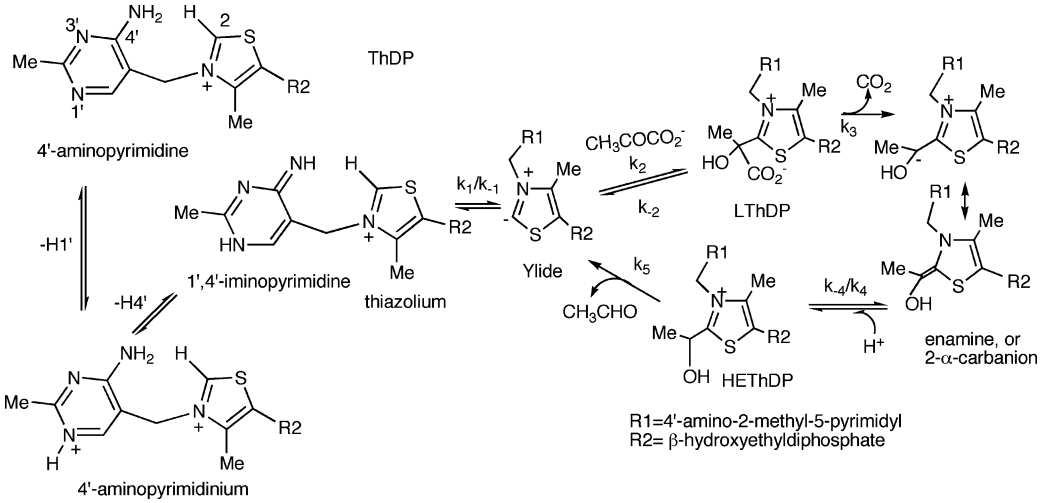

Table 1: Steady-State Kinetic Parameters for Wild-Type YPDC and the Loop 290−301 Variants at pH 6.0

YPDC variant	k_{cat} (s^{-1})	$S_{0.5}$ (mM)	n_H	$k_{cat}/S_{0.5}{}^n$ (mM^{-n} s^{-1}) or k_{cat}/A for WT (mM^{-2} s^{-1})	$k_{cat}/S_{0.5}$ (mM^{-1} s^{-1})	K_i (mM)
WT	37.54 ± 0.32	1.80 ± 0.05	1.66 ± 0.05	22.04 ± 1.85	20.81 ± 0.58	
D291A	0.0074 ± 2e-4	1.83 ± 0.13	1.25 ± 0.04	0.0034	0.0036 ± 2e−4	551.9 ± 135.5
N293A	0.0020 ± 7e-5	1.40 ± 0.11	1.31 ± 0.10	0.0013	0.0015 ± 1e−3	659.6 ± 432.2
T294A	0.24 ± 3.5e-3	15.34 ± 1.28	1.35 ± 0.05	0.0060	0.016 ± 1e−3	244.0 ± 46.8
S298A	1.23 ± 0.09	11.35 ± 1.39	1.34 ± 0.08	0.047	0.11 ± 0.03	272.7 ± 84.1
S300A	34.20 ± 0.56	1.16 ± 0.04	1.37 ± 0.06	27.99	29.56 ± 1.2	867.3 ± 288.2
D291N	0.0022 ± 0.001[a]					
ΔS296ΔF297	0.0016 ± 0.001[a]					

[a] From refs *11* and *12*.

Table 2: Kinetic Parameters Deduced from Activation Curves[a]

variant	v_0 (units/mg)	v_1 (units/mg)	v_2 (units/mg)	k_{tr1} (s^{-1})	k_{tr2} (s^{-1})
D291A	0	0.117 ± 0.078	0.0290 ± 0.0003	0.112 ± 0.079	0.113 ± 0.077
N293A	NA	0.00652 ± 0.00009	0.00872 ± 0.00012	NA	0.0436 ± 0.0062
T294A	0	2.90 ± 0.03	1.12 ± 0.01	0.917 ± 0.042	0.225 ± 0.003
S298A	NA	NA	7.17 ± 0.08	NA	0.140 ± 0.0038
S300A	0	23.8 ± 0.3	39.5 ± 0.4	NA	0.261 ± 0.0052
WT YPDC	0	9.65 ± 0.02	39.2 ± 0.4	NA	0.337 ± 0.0026

[a] The rates v_0, v_1, and v_2 represent steady-state rates of corresponding enzyme states E_0, E_1, and E_2 (Scheme 2). The transition rate constants k_{tr1} and k_{tr2} are associated with the transitions from E_0 to E_1 and E_1 to E_2. All experiments were carried out at pH 6.0. Data from Figures 4−9 were analyzed using eqs 3 and 4 as described in ref *15*. NA: Not apparent from curves hence not determined; where the numeral zero is inserted implies that the number was near zero and could not be determined with precision.

for T294A and S298A are increased 8- and 6-fold, respectively, suggesting that D291 and N293 may have functions in modulating the substrate binding.

Effects of Substitution on the Hill Coefficient. All variants showed modestly reduced positive cooperativity; the values of n_H are relatively smaller than those for wild-type YPDC in the entire pH range. Significantly, the cooperativity according to this criterion was not abolished in any of the loop variants.

(b) Steady-State Kinetic Analysis for Loop 104−113 Variant L111A (V/Q)

The steady-state kinetic parameters for the L111A(V/Q) variants in the pH range of 5.1−7.5 are listed in Supporting Information Tables S2.A−C with corresponding plots in Supporting Information Figures S2.A−C.

At pH 6.0, for the L111A, L111V, and L111Q respectively, the k_{cat} values are 47%, 21%, and 73% of that of the wild type; the $k_{cat}/S_{0.5}$ values are 18%, 3%, and 39% of that of the wild type; $k_{cat}/S_{0.5}{}^n$ values are 0.2%, 2%, and 5.8% of the k_{cat}/A of the wild type; $S_{0.5}$s were increased by 2.6-, 6-, and 1.9-fold. The n_Hs are virtually unaffected by the substitutions on the L111 position compared to the wild-type YPDC in the entire pH range.

(c) Stability of Loop Variants

Overall, the T_ms determined by differential scanning calorimetry (in °C) were little changed by the loop substitutions: wild-type YPDC (70.20), D291A (68.46), N293A (71.71), D294A (70.50), and S298A (69.67).

(d) Pre-Steady-State Kinetics of Substrate Activation

The rate constants deduced from these studies are summarized in Table 2.

Wild-type YPDC. At substrate saturation, the shape of the progress curve for wild-type YPDC was similar to the one

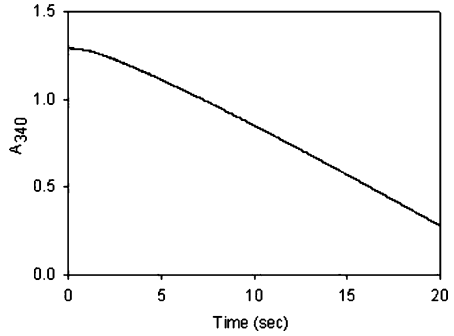

FIGURE 4: Progress curve for acetaldehyde formation by WT YPDC at the optimal pH of 6.00. WT YPDC (28 μg/mL) dissolved in MES buffer (pH 6.00) containing 35 units/mL of ADH, 0.46 mM NADH, 5 mM $MgCl_2$, and 2 mM ThDP was mixed in a 1:1 ratio with 100 mM pyruvate dissolved in MES (pH 6.00). Acetaldehyde release was monitored via the coupled assay.

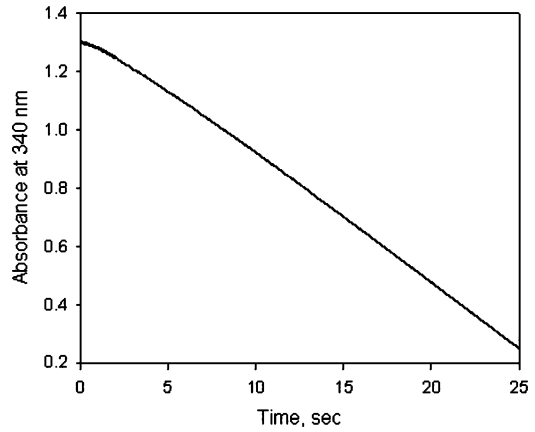

FIGURE 5: Progress curve for acetaldehyde formation by the S300A variant at pH 6.00. The S300A YPDC variant (22 μg/mL) dissolved in MES buffer (pH 6.00), containing 35 units/mL of ADH, 0.46 mM NADH, 5 mM $MgCl_2$, and 2 mM ThDP, was mixed in a 1:1 ratio with 100 mM pyruvate in MES (pH 6.00). Acetaldehyde release was monitored via the coupled assay.

Scheme 2: Two-Step Phenomenological Model of YPDC ([a]

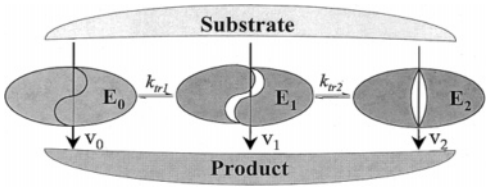

[a] Reference *15*.

reported earlier (*20*), with a lag phase and a steady state (Figure 4). Nonlinear regression analysis (SigmaPlot) enabled determination of the rate of both phases. The progress curves could be treated according to eq 4 assuming the existence of two enzyme conformations, E_1 and E_2, with corresponding distinct steady-state rates of v_1 and v_2 undergoing corresponding transitions $E_1 \rightarrow E_2$ as shown in Scheme 2. The value of the steady-state rate v_1 was smaller than of v_2.

S300A YPDC. The activity of S300A was similar to that of wild-type PDC. At substrate saturation, the shape of the progress curve for S300A was similar to that of wild-type YPDC with a lag phase and a steady state indicating the presence of two steady states and two corresponding enzyme conformations (Figure 5). Nonlinear regression treatment of the data indicated somewhat smaller v_1 than v_2, reminiscent of the behavior observed with the wild-type YPDC.

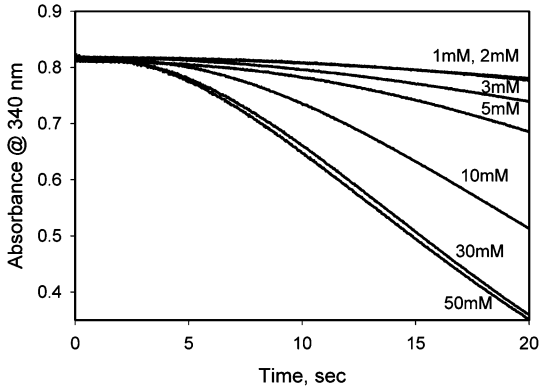

FIGURE 6: Progress curves for acetaldehyde formation by the S298A variant at pH of 6.00 at the indicated concentrations of pyruvate. The S298A YPDC variant (0.1 mg/mL) dissolved in 0.1 M MES buffer (pH 6.00), containing 35 units/mL of ADH, 0.46 mM NADH, 5 mM $MgCl_2$, and 2 mM ThDP, was mixed in a 1:1 ratio with pyruvate in MES (pH 6.00) resulting in the indicated concentrations of pyruvate. Acetaldehyde release was monitored via the coupled assay.

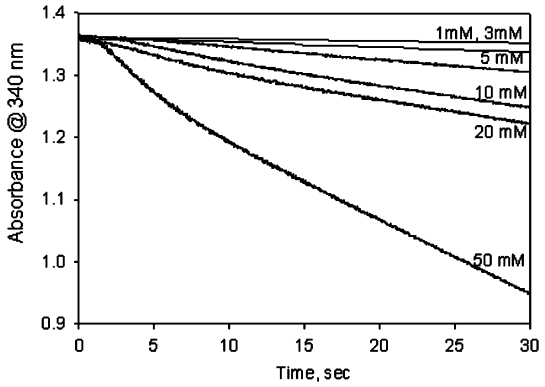

FIGURE 7: Progress curves for acetaldehyde formation by the T294A variant at pH 6.00. The T294A YPDC variant (0.2 mg/mL) dissolved in MES buffer (pH 6.00), containing 35 units/mL of ADH, 0.46 mM NADH, 5 mM $MgCl_2$, and 2 mM ThDP, was mixed in a 1:1 ratio with pyruvate in MES (pH 6.00) resulting in the indicated concentrations of pyruvate. Acetaldehyde release was monitored via the coupled assay.

S298A YPDC. The S298A variant is about 10 times slower than the wild-type YPDC, and it showed a similar progress curve as the wild-type and S300A variants indicating the existence of two enzyme conformations and two steady states (Figure 6). Nonlinear regression treatment of the data indicated negligible v_0 and v_1 compared with v_2 in this case.

T294A YPDC. The T294A is about 1000 times slower than the wild-type YPDC, and it showed a similar progress curve as the wild type at lower substrate concentration. However, at substrate saturation we could clearly observe three distinct steady-state rates (v_0, v_1, and v_2) suggesting three enzyme conformers undergoing consecutive transitions ($E_0 \rightarrow E_1 \rightarrow E_2$) (Figure 7). The first steady-state rate, v_0, is negligible compared to the second and third steady-state rates, v_1 and v_2. Data treatment enabled determination of the steady-state rates and the transition rate constants, k_{tr1} and k_{tr2} for enzyme conformational changes.

N293A YPDC. The N293A variant is approximately 10000-fold slower than the wild-type YPDC, and it showed a similar progress curve as the wild type at lower substrate concentration (Figure 8). However, at substrate saturation we could clearly observe two different steady-state rates (v_1

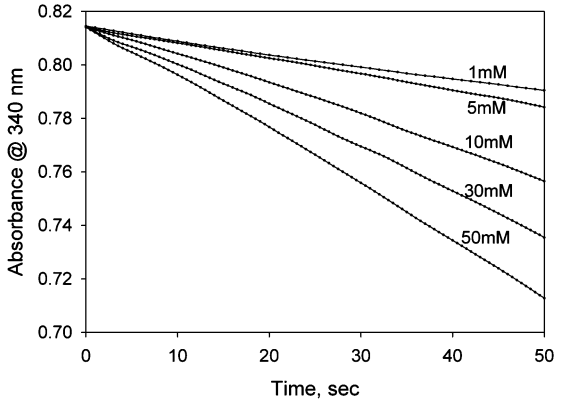

FIGURE 8: Progress curves for acetaldehyde formation by the N293A YPDC variant pH 6.00. The N293A YPDC variant (5 mg/mL) dissolved in MES buffer (pH 6.00), containing 35 units/mL of ADH, 0.46 mM NADH, 5 mM $MgCl_2$, and 2 mM ThDP, was mixed in a 1:1 ratio with pyruvate in MES (pH 6.00) resulting in the indicated concentrations of pyruvate. Acetaldehyde release was monitored via the coupled assay.

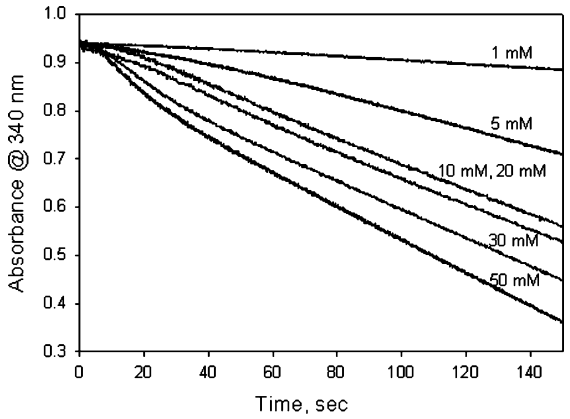

FIGURE 9: Progress curves for acetaldehyde formation by the D291A YPDC variant at pH 6.00. The D291A YPDC variant (2.3 mg/mL) dissolved in MES buffer (pH 6.00), containing 35 units/mL of ADH, 0.46 mM NADH, 5 mM $MgCl_2$, and 2 mM ThDP, was mixed in a 1:1 ratio with pyruvate in MES (pH 6.00) resulting in the indicated concentrations of pyruvate. Acetaldehyde release was monitored via the coupled assay.

and v_2) suggesting two enzyme conformers undergoing consecutive transitions ($E_1 \rightarrow E_2$) while lacking the lag phase. Data treatment enabled determination of the steady-state rates, v_1 and v_2, and the transition rate constants, k_{tr2}, for enzyme conformational change.

D291A YPDC. The D291A variant is approximately 10000-fold slower than the wild-type YPDC, and it showed a similar progress curve as the wild type at lower substrate concentration. Again, at substrate saturation we could clearly observe three distinct steady-state rates (v_0, v_1, and v_2) suggesting three enzyme conformers undergoing consecutive transitions ($E_0 \rightarrow E_1 \rightarrow E_2$) (Figure 9). The first steady-state rate, v_0, is negligible compared to the second and third steady-state rates, v_1 and v_2. Data treatment enabled determination of the steady-state rates and the transition rate constants, k_{tr1} and k_{tr2}, for enzyme conformation changes.

The results of these studies are summarized in Table 2.

(e) Intermediate Distribution at Steady State

Using the method of Tittmann and Hübner (*17*), the distribution of intermediates at steady state was determined for several loop variants leading to rate constants for the key reaction steps (Table 3). The premise of the method is that (a) all of these intermediates such as LThDP and HEThDP are stable on acid quench; and (b) the resonance corresponding to C6′-H has a different chemical shift in ThDP, LThDP, and HEThDP (see Scheme 1 for numbering and abbreviations) under acid quench conditions, hence these resonances could be integrated to provide levels of each intermediate under different conditions. The NMR-based intermediate analysis has shown that, for all cases studied, the HEThDP accumulated predominantly at steady state. This in turn implies that elimination of acetaldehyde from HEThDP is rate limiting for overall catalysis.

DISCUSSION

Two regions were well conserved in YPDC in a comparison of the amino acid sequence of YPDC with other ThDP dependent enzymes (*21*). One sequence stretches from residues 212 to 374 in the β domain, and the other is between residues 436 and 483 in the γ domain, implying the importance of these two regions in the ThDP cofactor binding and function. A common ThDP binding motif has been found in all ThDP-dependent enzymes (*21*−*23*). This region, comprising about 30 residues, starts from -GDG- and ends with -NN-. In YPDC, this motif spans residues G443−N471, within the scope of the γ domain conserved region. This region and the key active center residues have been explored thoroughly by several groups including our two groups. In this study, we explored the loop region from 290 to 301, which is located within a conserved region of the β domain.

Location and Potential Interactions of Loop 290−*301.* An inspection of the pyruvamide-activated YPDC crystal structure (form B) revealed that numerous interactions of this loop are involved, either directly or indirectly, with some other important residues such as (a) the regulatory site pivot C221, (b) residues involved in dimer−dimer assembly, (c) residues participating in the intraloop interactions, and (d) the active center residue H114 (*3*). These potential interactions are listed in Table 4.

First, the residue G286 is located four residues upstream from loop 290−301, and the distance of its backbone oxygen from the backbone nitrogen of C221 is 2.93 Å, the typical length of a hydrogen bond (Figure 2). Previous studies have suggested that C221 is the trigger in the substrate activation of YPDC. Based on the results of a series of studies of the regulatory sites, a putative activation pathway was proposed (*6*−*8*, *15*, *25*−*30*). Residues involved in this pathway include H92 and E91 from the α domain, C221 from the β domain, and V410, L411, W412, G413, and I415 from the γ domain, among which G413 and I415 provide two of the three conserved hydrogen bonds to the 4′-aminopyrimidine ring of the ThDP (the third one is E51). Upon pyruvate binding the signal from C221 is propagated through the pathway to the active center. This substrate activation pathway involves interactions among all three domains. Inhibition studies and model building had demonstrated that the interactions between the domains are balanced in a very delicate manner. Any disturbance could cause distortion of the active center as well as abolition of cooperativity (*25*, *28*). Substitution or deletions of the residues on the loop certainly changed

Table 3: Microscopic Rate Constants for the Loop Variants from Analysis of Intermediate Distribution

variant	k_{cat} (s^{-1})	k_2 (s^{-1}) C−C bonding	k_3 (s^{-1}) CO_2 release[b]	k_{45} (s^{-1}) acetaldehyde release
WT[a]	45 ± 2	294 ± 20	105 ± 6	105 ± 6
D291A	0.0075 ± 3e−4	0.0527 ± 2e−3	0.0450 ± 2e−3	0.0109 ± 4e−3
N293A	0.0307 ± 5e−3	0.842 ± 0.13	0.969 ± 0.16	0.0330 ± 5e−3
T294A	0.535 ± 0.07	4.86 ± 0.63	5.59 ± 0.89	0.674 ± 0.09
S298A	0.893 ± 0.05	10.2 ± 0.57	7.49 ± 0.42	1.13 ± 0.06

[a] Rate constants for pyruvate binding (k_2), decarboxylation (k_3), and the composite rate constant (see text) (k_{45}) as calculated by using the ^{1}H NMR intermediate distribution shown in Figure 10 using the method in ref *17*. [b] These values for the variants represent a lower limit on the rate constants in view of the low population of LThDP.

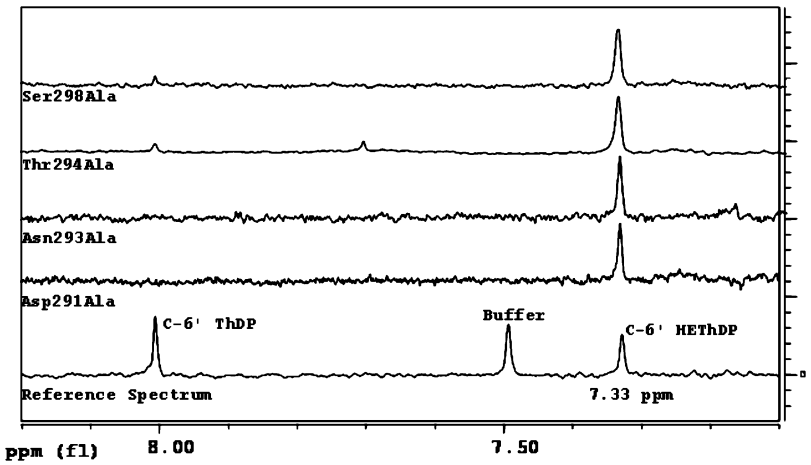

FIGURE 10: ^{1}H NMR determination of intermediate concentrations at steady state by YPDC and variants. Stacked ^{1}H NMR spectra display the chemical shift range of 7.10−8.20 ppm for intermediate distribution in steady state of acetaldehyde release from pyruvate (50 mM) using YPDC loop variants. The spectra were recorded at pH 0.75 with D_2O as the solvent using a Varian 500 MHz spectrometer. The reaction mixture was acid-quenched at 2−3 half-lives of the reaction, centrifuged, and filtered with a 0.45 μm filter to isolate the intermediates. Qualitative analysis was performed using the chemical shift of the C6′-H signal of the ThDP analogue of the intermediate, and quantitative analysis was done with the integration of the relative C6′-H integrals (*17*). Resonance at 7.7 ppm with the Thr294Ala variant is of unknown origin.

Table 4: Possible Interactions in Which the Loop 290−301 Might Be Involved

interaction categories	possible interactions[a] residue. atom−residue. atom	distance (Å)
dimer−dimer	D291 (A). OD−K304 (C). NZ	3.3 (3.6)
	D291 (A). OD−N318 (C). ND	3.8 (4.6)
	D291 (A). OD−N318 (C). OD	4.2
	N293 (A). ND−N318 (C). O	3.5
	N293 (A). OD−N318 (C). ND	4.3
	S300 (A). OG−N318 (C). ND	3.5
	S300 (A). OG−N318 (C). OD	4.9
	S300 (A). OG−K304 (C). NZ	3.8
intraloop	D291 (A). OD−S300 (A). OG	3.1 (2.8)
	D291 (A). OD−Y301(A). N	3.3 (4.9)
	N293 (A). OD−S298 (A). OG	3.4
	N293 (A). OD−Y299 (A). N	4.4
	N293 (A). OD−F 297(A). O	4.9
	N293 (A). ND−S298 (A). OG	4.5
with active center	T294 (A). OG−H114 (B). ND	4.1

[a] Letters in the parentheses (A, B, C, and D) represent different subunits: A and C are C-subunits, and B and D are O subunits. O: backbone oxygen. N: backbone nitrogen. OD: delta oxygen. ND: delta nitrogen. OG: gamma oxygen. NZ: epsilon nitrogen.

the loop properties. Since G286 is only 4 residues away from the loop, these loop substitutions would also affect the H-bond interaction between G286 and C221. This perturbation alters the position of residue C221 and somehow weakens its pivotal functions in both substrate activation and domain−domain interactions. The smaller Hill coefficients of all loop variants compared to that of the wild-type YPDC are consistent with the diminished positive cooperativity.

Second, the loop itself folds into a hairpin conformation with a few intraloop interactions (Figure 3, Table 4), implying a highly organized and stable structure. In fact, the loop has a well-defined secondary structure that consists of two antiparallel β-strands and has close contact with another loop, 104−113 from the open subunit. Both loops fold over and create a closed conformation for the two active centers in the closed form subunits (Figure 1). On the other hand, the remaining two active sites in the open subunits with the corresponding loops disordered are in an open conformation and are accessible to the solvent. No important interactions were revealed by the X-ray structure around residues S296 and F297. Deletion of these two residues results in a nearly inactive enzyme, suggesting that the length and the correct folding (or proper conformation) of the loop are essential to enzyme function.

Third, loop 290−301 is stabilized only upon the binding of the substrate or substrate analogue, as a more closely contacted interface is formed between the two C-subunits. Therefore, a plausible conjecture is that the loop plays an important role in the formation of the asymmetric active tetramer. Two residues from one C-subunit, K304 and N318, are found to closely interact with D291, N293, and S300 in the loop of the opposite C-subunit and vice versa (Table 4). Substrate activation of the YPDC involves a major tetramer

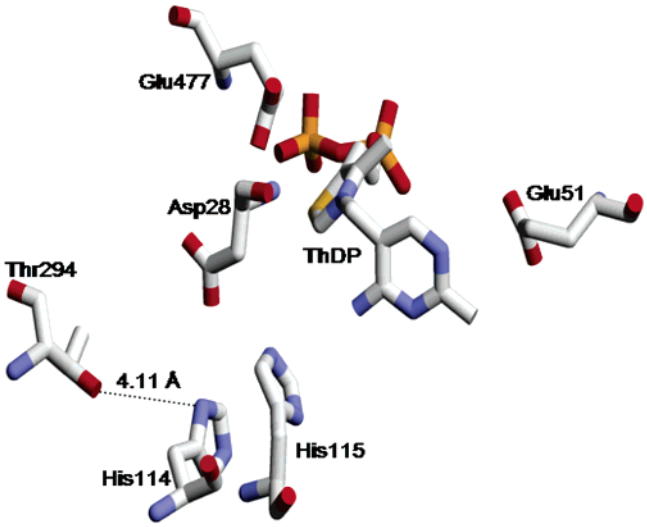

FIGURE 11: Loop residue T294 and its proximity to residue H114 and other active-site residues with the coenzyme ThDP. The pdb file 1qpb (ref *3*) was used to generate the model.

structural rearrangement. The dimer−dimer interface between the two closed form subunits is much larger than in the unactivated form (form A). The importance of this conformational change, which leads to an active enzyme, was demonstrated (*31*, *32*). The interactions between K304, N318, and the loop from the opposite subunit are probably among the numerous packing interactions on the dimer−dimer interface and are critical in the form B structure.

Deductions from Steady-State Kinetics. The results of the steady-state measurements for the loop 290−302 variants show dramatic decrease in both k_{cat} and $k_{cat}/S_{0.5}$ (except those for S300A), in spite of the fact that these variant enzymes were highly expressed in *E. coli* to a level comparable to wild-type enzyme. In a previous study, two other variants, *pdc1−8* (D291N) and *pdc1−803* (S296ΔF297Δ) were created (*11*, *12*). The k_{cat}s determined for *pdc1−8* and *pdc1−803* were 0.0022 and 0.0016, respectively (*11*, *12*). As this loop is not directly involved in the active center environment, and may or may not participate in the substrate-activation mechanism, the approximately 20000-fold lower activities found in D291A, N293A, *pdc1−8*, and *pdc1−803* in comparison with wild-type YPDC are so far the lowest activities detected among all the YPDC variants studied in our laboratories. This includes the active center variants (*13*, *24*) and the variants along the putative substrate-activation pathway leading from C221 to ThDP (*7*, *8*, *25*). Therefore, substitutions at these specific sites not only cause disturbances of local interactions but also induce a conformational distortion of the entire enzyme structure. This altered conformation could affect the enzyme function in several respects, such as formation of the functional tetramer, binding of the ThDP cofactor, protection of the active center environment, etc.

Finally, the interaction between the gamma oxygen of T294 and the delta nitrogen of H114 is indicated by the crystal structure (Figures 2 and 11). The role of H114 as an acid−base group at the active center is confirmed (*13*, *17*). The residue H114 is one of the two histidines (the other one is H115) that were found to be essential in the substrate binding in the YPDC and PDC from *Zymomonas mobilis* (the corresponding histidines are H113 and H114) (*13*, *23*). The $S_{0.5}$ for T294A is 15.3 mM at pH 6.0, greater than those of any other variants (Table 1). The results of the kinetic analysis and an examination of the crystal structure suggest the impact of the loop 290−301 on the active center and also confirm the important role H114 plays in the substrate binding.

The steady-state results for the L111 variants are not very dramatic, hence no firm conclusion could be reached concerning this residue or the loop 104−113.

Deductions from Substrate Activation Progress Curves and Intermediate Trapping Studies. The evidence for existence of three conformers of YPDC has been reinforced by the study of the flexible loop variants. The residue S300 does not form any hydrogen bond while the main-chain oxygen of S298 forms a hydrogen bond with the nitrogen of T266. The nitrogen of S298 also participates in an intraloop hydrogen bond with the oxygen of F292.

Substitution of S298 could cause a minor alteration in the residue's hydrogen-bonding pattern leading to diminished activity. While not altering the substrate activation behavior, the diminished activity induced by the S298A substitution is the result of a reduced product release rate according to the ^{1}H NMR study. Both the S300A and S298A variants behave similarly to the wild-type YPDC at pH 6.00 so far as substrate activation is concerned. The other variants displayed anomalous activation behavior even at pH 6.00, reminiscent of the behavior displayed by the wild-type YPDC at pH 5.0 (*15*) and reported from Halle on the pyruvate decarboxylase from *Kluveromyces lentis* (*16*). Substrate saturation is required to observe the three steady-state rates for the T294A and D291A variants. The N293A variant behaves differently from any of the other enzyme forms, essentially eliminating substrate activation and giving rise to two conformers at pH 6.00.

The main-chain oxygen of T294 forms an intraloop hydrogen bond with the nitrogen of F297 (3.37 Å) while the nitrogen of T294 forms a hydrogen bond with the oxygen of F297 (2.86 Å). In addition to these intraloop bonds, T294 also participates in van der Waals interactions with the active-site residue H114 (4.11 Å, Figures 2 and 11), located adjacent to H115. Variants of both of these residues resulted in drastic reduction of YPDC activity (*13*), while corresponding residues of PDC from *Zymomonas mobilis* were shown to participate primarily in post-decarboxylation steps according to the intermediate distribution studies (*17*). Both of these residues participate in hydrogen bonds with residues along the putative activation pathway. The H114 is H-bonded to V410 (2.87 Å) and L411 (3.64 Å), while His115 is H-bonded to L411 (3.06 Å), W412 (3.58 Å), and G413 (3.37 Å).

We had seen above that the T294A variant has a considerably reduced activity displaying a substrate activation behavior similar to that for wild-type YPDC at pH 5.0, suggesting the presence of three enzyme states. Since with this variant the interaction with His114 is affected, consequently the entire activation pathway could be affected. This cascade of effects would not only disrupt the activation pathway but could also affect the activity by hindering the release of the product as shown by the steady-state rapid-quench ^{1}H NMR studies.

The main-chain nitrogen of N293 forms two intraloop H-bonds, one with the oxygen of F297, the other with the main-chain oxygen of Y299. In the open, "O", form of the

functional dimer, the side-chain nitrogen of this residue forms an unusual H-bond with the oxygen of L111, which is a part of the second loop not seen in the "nonactivated" structure. Yet, as discussed above, substitution of residue L111 did not significantly affect the activity.

The residue N293 forms a H-bond (2.99 Å) with T294 in the "O" form. These interactions could play a pivotal role in the activation process as well as the final product release step since the N293A substitution drastically lowered the activity and did not show the first step of activation, instead revealing the other two steady-state steps.

The nitrogen of residue D291 forms an intraloop H-bond with the main-chain oxygen of Y299. As does the N293A substitution, the D291A substitution leads to a drastic reduction in activity but still shows the presence of three enzyme states in the pre-steady-state activation study. Unlike the residue N293, D291 does not participate in any special H-bond interactions for this residue in the open conformation. Only the above-mentioned H-bond interactions would have an effect on the activation process since D291 is just four residues away from G286, implying that the D291A substitution affects the H-bond between G286 and C221, resulting in the change in the activation process and also affecting the rate of product release.

The mathematical treatment of the data required two exponentials with a linear part. Earlier, a detailed study of the progress curve for wild-type YPDC (*15*) in a broad pH range showed the presence of two transitions and only the steady-state rates were subject to change. They suggested the existence of three enzyme conformations (denoted as E_0, E_1, and E_2) characterized by three distinct steady-state rates (v_0, v_1, and v_2), connected by two steps ($E_0 \rightarrow E_1 \rightarrow E_2$).

The previous model for YPDC activation suggested the presence of two enzyme states based on the data at the optimal pH of 6.0 (*19*, *20*). There, the unregulated enzyme was considered to be inactive and the transition from the unregulated and regulated state was suggested to represent a slow reversible conformational change after the substrate-binding step at the regulatory site.

Since we have observed the first enzyme state E_0 to be inactive in all of the loop variants except N293A, which seems to lack the E_0 state completely, we will discuss the other two enzyme states E_1 and E_2 and their corresponding transitions k_{tr1} and k_{tr2}. The study by Sergienko and Jordan (*15*) suggested that the first transition, k_{tr1}, corresponds to substrate binding at the active site since an increase in the ES complex formation at lower pH values was observed. This suggestion was supported by a plausible accounting of the pH dependence: substrate binding at the regulatory site should not increase with lowering of pH, since the putative trigger C221 would have a smaller fraction in the reactive $C221S^-$ form (to form a hemithioketal with pyruvate) at lower pH. The second enzyme state E_1 in the variants arises after the binding of the substrate at the active site while the third enzyme state E_2 usually referred to as the regulated enzyme arises after the binding of a pyruvate molecule at the regulatory site (*15*), which is associated with the rate constant k_{tr2}. Earlier accounts pertaining to this transition were deduced from the fact that this transition exhibited saturation with substrate indicating an enzyme−substrate complex and the inability of pyruvate to access the active site which already has a pyruvate molecule (*15*). As we would expect, the least active N293A variant though lacking the initial activation step has the lowest k_{tr2} value.

SUMMARY AND CONCLUSIONS

To summarize, loop 290−301 functions in substrate activation as well as in catalysis. According to the Hill coefficient as a criterion of substrate activation, with most loop variants the substrate activation is diminished but not abolished, hence the results do not rule out C221 as the trigger for substrate activation, notwithstanding the implications of the structure of the pyruvamide-activated YPDC (*3*). The integrity and the correct conformation of the loop are essential in the proper enzyme functioning. The loop takes part in the new dimer−dimer interface formation in form B YPDC.

The catalytic activity of the S298A and S300A variants is at par with that of the wild-type YPDC at the optimal pH value of 6.0. The D291A and T294A variants have very low activity and behave like the wild-type enzyme at lower pH values as we can see two transitions and three enzyme states even at optimal pH. The extremely low activity mutant, N293A, does not display the initial lag phase observed with the other variants emphasizing a perturbed conformation in its original state. The stopped-flow study on activation provides further support for the phenomenological model of YPDC involving multiple conformational states. The steady-state intermediate distribution study clearly shows that the release of acetaldehyde is slowed down in all variants and is the rate-limiting step in the sequence of reactions in Scheme 1.

Finally, we note that, with the advent of large numbers of related protein sequences in the databases, it is clear that this region of the β domain is conserved in quite a few species, as is the C221/H92 combination, suggesting that the results on YPDC should be applicable to a number of related pyruvate decarboxylases.

ACKNOWLEDGMENT

E.J. wishes to acknowledge helpful discussions with Eduard Sergienko regarding the treatment of pre-steady-state kinetics.

SUPPORTING INFORMATION AVAILABLE

Eight sets of figures and tables on the steady-state kinetic data collected in the entire pH range of activity for the D291A, N293A, T294A, S298A, S300A, L111A, L111V, and L111Q YPDC variants. This material is available free of charge via the Internet at http://pubs.acs.org.

REFERENCES

1. Dyda, F., Furey, W., Swaminathan, S., Sax, M., Farrenkopf, B., and Jordan, F. (1993) Catalytic Centers in the Thiamin Diphosphate Dependent Enzyme Pyruvate Decarboxylase at 2.4Å Resolution, *Biochemistry 32*, 6165−6170.
2. Arjunan, P., Umland, T., Dyda, F., Swaminathan, S., Furey, W., Sax, M., Farrenkopf, B., Gao, Y., Zhang, D., and Jordan, F. (1996) Crystal structure of thiamin diphosphate-dependent enzyme pyruvate decarboxylase from the Yeast *Saccharomyces cerevisiae* at 2.3 Å resolution, *J. Mol. Biol. 256*, 590−600.
3. Lu, G., Dobritzsch, D., Baumann, S., Schneider, G., and König, S. (2000) The structural basis of substrate activation in yeast pyruvate decarboxylase, *Eur. J. Biochem. 267*, 861−868.

4. Boiteux, A., and Hess, B. (1970) Allosteric properties of yeast pyruvate decarboxylase, *FEBS Lett. 9*, 293−296.
5. Ullrich, J., and Donner, I. (1970) Kinetic evidence for two active sites in cytoplasmic yeast pyruvate decarboxylase, *Hoppe-Seyler's Z. Physiol. Chem. 351*, 1026−1029.
6. Baburina, I., Gao, Y., Hu, Z., Jordan, F., Hohmann, S., and Furey, W. (1994) Substrate Activation of Brewers' Yeast Pyruvate Decarboxylase Is Abolished by Mutation of Cysteine 221 to Serine, *Biochemistry 33*, 5630−5635.
7. Li, H., Furey, W., and Jordan, F. (1999) Role of glutamate 91 in information transfer during substrate activation of yeast pyruvate decarboxylase, *Biochemistry 38*, 9992−10003.
8. Li, H., and Jordan, F. (1999) Effects of Substitution of Tryptophan 412 in the Substrate Activation Pathway of Yeast Pyruvate Decarboxylase, *Biochemistry 38*, 10004−10012.
9. Jordan, F. (2003) Current mechanistic understanding of thiamin diphosphate-dependent enzymatic reactions, *Nat. Prod. Rep. 20*, 184−201.
10. Eberhardt, I., and Hohmann, S. (1995) Strategy for deletion of complete open reading frames in *Saccharomyces cerevisiae*, *Curr. Genet. 27*, 306−308.
11. Eberhardt, I., Cederberg, H., Li, H., König, S., Jordan, F., and Hohmann, S. (1999) Autoregulation of yeast pyruvate decarboxylase gene expression requires the enzyme but not its catalytic activity, *Eur. J. Biochem. 262*, 191−201.
12. Li, H. (1999) Ph.D. Thesis, Rutgers University.
13. Liu, M., Sergienko, E. A., Guo, F., Wang, J., Tittmann, K., Hübner, G., Furey, W., and Jordan, F. (2001) (2001) Catalytic Acid-Base Groups in Yeast Pyruvate Decarboxylase. 1. Site-Directed Mutagenesis and Steady-State Kinetic Studies on the Enzyme with the D28A, H114F, H115F, and E477Q Substitutions, *Biochemistry 40*, 7355−7368.
14. Holzer, H., Schultz, G., Villar-Palasi, C., and Jutgen-Sell, J. (1956) Isolierung der hefecarboxylase and untersuchunger uber die activitat des enzymes in lebenden zellen, *Biochem. Z. 327*, 331−344.
15. Sergienko, E. A., and Jordan, F. (2002) A New Model for Activation of Yeast Pyruvate Decarboxylase by Substrate Consistent with the Alternating Sites Mechanism: Demonstration of the Existence of Two Active Forms of the Enzyme, *Biochemistry 41*, 3952−3967.
16. Krieger, F., Spinka, M., Golbik, R., Hübner, G., and König, S. (2002) Pyruvate decarboxylase from *Kluyveromyces lactis*. An enzyme with an extraordinary substrate activation behavior, *Eur. J. Biochem. 269*, 3256−3263.
17. Tittmann, K., Golbik, R., Uhlemann, K., Khailova, L., Schneider, G., Patel, M., Jordan, F., Chipman, D. M., Duggleby, R. G., and Hübner, G. (2003) NMR Analysis of Covalent Intermediates in Thiamin Diphosphate Enzymes, *Biochemistry 42*, 7885−7891.
18. Wei, W. (2003) Ph.D. Thesis Rutgers University.
19. Alvarez, F. J., Ermer, J., Hübner, G., Schellenberger, A., and Schowen, R. L. (1995) The linkage of catalysis and regulation in enzyme action. Solvent isotope effects as probes of protonic sites in the yeast pyruvate decarboxylase mechanism, *J. Am. Chem. Soc. 117*, 1678−1683.
20. Hübner, G., Weidhase, R., and Schellenberger, A. (1978) The mechanism of substrate activation of pyruvate decarboxylase: a first approach, *Eur. J. Biochem. 92*, 175−181.
21. Green, J. B. **(**1989) Pyruvate decarboxylase is like acetolactate synthase (ILV2) and not like the pyruvate dehydrogenase E1 subunit, *FEBS Lett.* 246, 1−5.
22. Hawkins, C. F., Borges, A., and Perham, R. N. (1989) A common structural motif in thiamin pyrophosphate-binding enzymes, *FEBS Lett. 255*, 77−82.
23. Candy, J. M., and Duggleby, R. G. (1998) Structure and properties of pyruvate decarboxylase and site-directed mutagenesis of the *Zymomonas mobilis* enzyme, *Biochim. Biophys. Acta 1385*, 323−338.
24. Gao, Y. (2000) Ph.D. Thesis, Rutgers University.
25. Baburina, I., Li, H., Bennion, B., Furey, W., and Jordan, F. (1998) Interdomain information transfer during substrate activation of yeast pyruvate decarboxylase: the interaction between cysteine 221 and histidine 92, *Biochemistry 37*, 1235−1244.
26. Zeng, X., Farrenkopf, B., Hohmann, S., Dyda, F., Furey, W., and Jordan, F. (1993) Role of cysteines in the activation and inactivation of brewers' yeast pyruvate decarboxylase investigated with a PDC1-PDC6 fusion protein, *Biochemistry 32*, 2704−2709.
27. Baburina, I., Moore, D. J., Volkov, A., Kahyaoglu, A., Jordan, F., and Mendelsohn, R. (1996) Three of Four Cysteines, Including That Responsible for Substrate Activation, Are Ionized at pH 6.0 in Yeast Pyruvate Decarboxylase: Evidence from Fourier Transform Infrared and Isoelectric Focusing Studies, *Biochemistry 35*, 10249−10255.
28. Baburina, I., Dikdan, G., Guo, F., Tous, G. I., Root, B., and Jordan, F. (1998) Reactivity at the substrate activation site of yeast pyruvate decarboxylase: inhibition by distortion of domain interactions. *Biochemistry 37*, 1245−1255.
29. Wang, J., Golbik, R., Seliger, B., Spinka, M., Tittmann, K., Hübner, G., and Jordan, F. (2001) Consequences of a Modified Putative Substrate-Activation Site on Catalysis by Yeast Pyruvate Decarboxylase, *Biochemistry 40*, 1755−1763.
30. Wei, W., Liu, M., and Jordan, F. (2002) Solvent kinetic isotope effects monitor changes in hydrogen bonding at the active center of yeast pyruvate decarboxylase concomitant with substrate activation: the substituent at position 221 can control the state of activation, *Biochemistry 41*, 451−461.
31. König, S., Hübner, G., and Schellenberger, A. (1990) Cross-linking of pyruvate decarboxylase. Characterization of the native and substrate-activated enzyme states, *Biomed. Biochim. Acta 49*, 465−471.
32. Hübner, G., König, S., Schellenberger, A., and Koch, M. H. (1990) An X-ray solution scattering study of the cofactor and activator induced structural changes in yeast pyruvate decarboxylase (PDC), *FEBS Lett. 266*, 17−20.

BI0615588